This article has been accepted for publication in a future issue of this journal, but has not been fully edited. Content may change prior to final publication. Citation information: DOI 10.1109/JESTPE.2014.2331062, IEEE Journal of Emerging and Selected Topics in Power Electronics

Reduced-Order Electrochemical Model Parameters Identification and SOC Estimation for Healthy and Aged Li-Ion Batteries

Part II: Aged Battery Model and State of Charge Estimation

Ryan Ahmed, Mohammed El Sayed, Ienkaran Arasaratnam, Jimi Tjong, Saeid Habibi

Abstract— **Recently, extensive research has been conducted in the field of battery management systems due to increased interest in vehicles electrification. Parameters such as battery state of charge and state of health are of critical importance to ensure safety, reliability, and prolong battery life. This paper includes the following contributions: (1) tracking reduced-order electrochemical battery model parameters variations as battery ages, using non-invasive genetic algorithm optimization technique, (2) the development of a battery aging model capable of capturing battery degradation by varying the effective electrode volume, (3) estimation of the battery critical state of charge using a new estimation strategy known as the Smooth Variable Structure Filter based on reduced-order electrochemical model. The proposed filter is used for state of charge estimation, and demonstrates strong robustness to modeling uncertainties which is relatively high in case of reduced-order electrochemical models. Batteries used in this research are lithium-Iron Phosphate cells widely used in automotive applications. Extensive testing using real-world driving cycles are used for estimation strategy application and for conducting the aging test. Limitations of the proposed strategy are also highlighted.**

Index Terms— Lithium-Ion Batteries, electrochemical battery model, state of charge estimation, state of health estimation, smooth variable structure filter.

I. INTRODUCTION

THIS paper involves the identification of the reduced-order electrochemical model parameters based on aged batteries, in addition to the application of a battery state of charge (SOC) estimation strategy. The paper presents an extension to [1], in which battery model parameters for fresh batteries are obtained using genetic algorithm. Furthermore, an aging model has been developed by changing the effective volume of the electrode to accommodate for battery aging. This section includes research motivation, peak oil concept, literature review of battery state of charge estimation techniques, significant paper research contributions, and the paper outline.

A. Motivation and Technical Challenges

Battery SOC and state of health (SOH) estimation represent a challenging task, since the traction battery exhibits fast changing dynamics due to acceleration and deceleration depending on the driving cycle. In order to ensure a reliable electric vehicle performance, precise estimation of lithium-Ion battery SOC and S[1]OH is crucial [2]. SOC is defined as the remaining pack capacity thus provides an indication of the vehicle remaining range [3]. SOH is a measure of the irreversible degradation that occurs in the battery performance due to cycling [3]. The current state of the battery is compared to that of the fresh battery (before cycling) [3]. SOH is a measure of the battery capability to respond to the required power demand and alarm if maintenance is required. Accordingly, an accurate estimation of the battery SOH is crucial to the battery operation [3]. In general, two main critical factors are considered when addressing the battery SOH, namely: capacity fade and power capability. The battery capacity fade has a huge impact on the vehicle range associated with customer range anxiety. The second factor is the power capability which impact the vehicle performance and drivability. The remaining useful life (RUL) is used to predict the battery remaining useful time during its life time thus it represents a proactive act for battery maintenance [3].

Battery SOC and SOH are highly correlated, a trade-off exists between extending the life-time of the battery and extending the range of the vehicle [2]. Discharging the battery to a high level of depth of discharge (DOD) (i.e.: low SOC) is generally not recommended as it will significantly shorten the lifetime of the battery. However, this will lead to shorter driving range as only partial charge is being utilized from the entire stored charge. In contrast, charging the battery beyond the acceptable range of operation results in high temperature and shortens the battery life [2]. Consequently, an accurate SOC estimate is of utmost importance in electric vehicles; any deviation in SOC estimation might result in an irreversible loss of capacity or even battery permanent damage [2].

Since electric and hybrid vehicles have been recently introduced to the market, it will require some time to assess their performance in real world operation. In particular, the battery might suffer from irreversible degradation due to cycling and that will adversely affects the SOC estimation accuracy which is of great concern to the driver. The Battery management system (BMS) has to be adaptive in order to account for aging and degradation in performance that might affect the vehicle range of operation and charging efficiency.

Manuscript received December 1, 2013; revised January 30, 2014; accepted April 30, 2014. The review of this paper was co-ordinated by R. Ahmed.

R. Ahmed, M. El Sayed, I. Arasaratnam and S. Habibi are with the Department of Mechanical Engineering, McMaster University, Hamilton, ON L8S4L7, Canada(e-mail: ryan.ahmed@mcmaster.ca; abugabma@mcmaster.ca, haran@ieee.org, habibi@mcmaster.ca).

J. Tjong is with Ford Motor Company of Canada, Windsor, ON N8Y 1W2 (jtjong@ford.com).

This article has been accepted for publication in a future issue of this journal, but has not been fully edited. Content may change prior to final publication. Citation information: DOI 10.1109/JESTPE.2014.2331062, IEEE Journal of Emerging and Selected Topics in Power Electronics

For instance, as per October, 2012, there are 112 documented cases of customers complaining of capacity loss in their electric vehicles [4]. In addition, around 11.8% of the total number of Nissan Leaf vehicles sold in Arizona have exhibited a loss in capacity gauge bars (Note: first capacity bar represents 15% capacity loss and 6.25 in the subsequent bars) [4].

B. Literature Review

Adaptive techniques for SOC estimation are extremely important especially for automotive applications where having an accurate, reliable, and robust estimate is necessary to mitigate the driver range anxiety concerns and ensure safety. In the literature, adaptive SOC estimation techniques are classified to one of the following: Fuzzy Logic, Artificial Neural Networks, and filter/observer-based techniques (such as Kalman Filters). The work in this paper will focus on filter/observer based methods.

In [5], using Kalman filter, a SOC, potentials, and concentration gradients estimation strategy based on reduced-order electrochemical battery model is presented. Estimates are compared against experimental data from a 6 Ah electric vehicle battery cell [5]. The filter provides accurate and stable estimates for low current input values. However, at very high C-rates that leads to near electrode maximum or minimum concentrations, the estimates exhibit large errors [5]. The filter used in this research has 4-7 states which is of relatively low order compared to equivalent circuit-based models [5]. The presented technique is computationally efficient to run in real-time applications such as an on-board battery management system [5].

In [6], a state estimation based on an output error injection observer using a reduced set of partial differential algebraic equations describing the solid and electrolyte concentrations and potentials is presented. Simulation and experimental results using real-world driving cycles such as the urban dynamometer driving schedule (UDDS) demonstrate the effectiveness of the proposed technique. In [7], a state of charge estimation technique based on a linearized battery model is presented. In order to overcome the nonlinear behavior of battery models, the Open circuit voltage-State of charge (OCV-SOC) relationship has been divided into linear sections and model parameters are estimated for each section individually [7]. Then based on the resultant linear model, an observer has been applied to estimate the state of charge. The technique has been verified using 1.5 Ah lithium-polymer cells [7].

C. Contributions

From the literature, most electrochemical based models did not account for aging and degradation effects which make them viable for fresh, healthy batteries only. However, as these batteries age with time, these models are not accurate and the SOC estimator might suffer from divergence and instability problems. Accordingly, developing an adaptive model that can account for cycling effects is of utmost importance. In addition, developing an adaptive model can significantly enhance the existing SOH estimation techniques and can provide an estimate for the battery RUL. Unlike most of the literature published to date, most papers that involve reduced-order electrochemical models are not fitted to experimental data with SOC estimation, besides, aging effects are generally not accounted for. Furthermore, tracking the electrochemical model parameters as battery degrades is crucial, since keeping track of these parameters that contribute to aging such as diffusion coefficient, solid-electrolyte interface resistance, and the OCV-SOC relationship can help in providing an adaptive, high fidelity model.

In this paper, electrochemical model parameters for aged batteries are estimated. An extensive accelerated aging test has been conducted on battery cells at high depth of discharge and elevated temperatures. The aging test continues until the battery reaches the battery end-of-life (80% of its capacity). Then a reference performance test using driving cycles has been conducted on aged batteries. The paper presents an aging model that can account for battery degradation at various battery states of life. The model works by varying the effective electrode volume, OCV-SOC relationship, solid-electrolyte interface resistance, and the solid diffusion coefficient thus account for aging. The model can be practically implemented in a real-time microprocessor for terminal voltage and state of charge estimation.

Finally, a battery critical surface charge estimation strategy has been designed to estimate the state of charge based on the identified battery model parameters. A strategy known as the Smooth Variable Structure Filter (SVSF) has been presented for battery critical surface charge estimation. The proposed strategy has been selected since it demonstrates robustness to modeling uncertainties, sensor noise, and to state of charge initial conditions [8, 9].

D. Paper Outline

This paper is organized as follows: section II involves a summary of the aging experiments conducted for experimental data generation. Section III includes battery aging model development in addition to model parameters identification for aged batteries. Section IV includes the application of state of charge estimation and the critical surface charge using the Smooth Variable Structure Filter (SVSF). Section V presents conclusions and limitations of the proposed strategy.

II. AGING/REFERENCE PERFORMANCE TEST EXPERIMENTS

Battery test procedures might vary depending on the country and the application, i.e.: for HEVs, PHEV, or EVs [10]. In this research, focus on test procedures used for PHEVs and EVs is attained. In U.S., battery test procedures are generally classified into 3 main categories: characterization, life, and reference tests [11].

1. *Characterization tests* are conducted to specify battery cell/pack baseline performance characteristics [11]. Examples of these tests include: static capacity, hybrid pulse power characterization (HPPC), self-discharge, cold cranking, thermal performance, and efficiency tests [11].
2. *Life tests* are conducted to determine battery degradation (aging) effects that take place in both cycle life and calendar life [11]. Calendar life means the life of the battery during storage (with no cycling involved) while cycle life is the life of the battery after multiple charging/discharging cycles [10]. The main purpose of

This article has been accepted for publication in a future issue of this journal, but has not been fully edited. Content may change prior to final publication. Citation information: DOI 10.1109/JESTPE.2014.2331062, IEEE Journal of Emerging and Selected Topics in Power Electronics

these tests is to perform an accelerated battery aging by acquiring data in a relatively short time therefore be able to predict the performance of the battery cell in practice. In addition, these tests can be used for battery warranty estimates.

3. *Reference performance tests (RPT):* are conducted periodically to track changes that might occur in the battery baseline characteristics. Reference tests are performed after conducting a certain number of life tests to measure the capacity fade and degradation in performance through the entire progress of battery life cycle [12]. In addition, these tests are performed at the beginning (fresh battery) and at the end of life state.

In this paper, a series of the aforementioned experiments have been conducted on 3 LiFePO4 battery cells. Characterization/RPT tests have been conducted at two different states of life, namely: fresh battery (at 100% capacity) and at 80% capacity. In the following subsection, a summary of tests conducted is this study.

A. Characterization/RPT tests

Extensive characterization tests have been conducted on a fresh and aged batteries at controlled room temperature of 25℃, 4 main experiments include: A static capacity test at 1C rate, SOC-OCV characterization test, and a driving scenario. The scenario includes a mix of driving schedules of an average North American driver, data generated is used to validate the accuracy of the SOC estimator and the aging model. A detailed description of the reference performance tests (ex: OCV-SOC, static capacity test) in addition to the experimental setup used in data generation can be found in part I of this paper [1].

Fast Charge/Discharge Aging (Life) Tests

Aging test using well-defined charging/discharging cycles at elevated temperature (55℃) and high C-rates have been conducted. The accelerated test has been conducted to track changes in battery electrochemical model parameters. Tests have been conducted on a 24/7 basis over a period of 3-6 months. The test procedure is as follows:

1. *Fully charge the battery in a CCCV mode until maximum voltage (3.6V).*
2. *Fully discharge the battery at constant current (CC) mode with 1C-rate until the voltage hits the minimum voltage (2V).*
3. *All cycler current accumulators are reset to zero. At this moment, the battery is at zero state of charge (SOC).*
4. *Charge the battery to 90% SOC.*
5. *Discharge the battery at 10 C-rate until the battery hits the minimum voltage (2V)*
6. *Allow for voltage relaxation for 5 minutes.*
7. *Charge the battery at 4C-rate for 20 minutes. If the battery hits the maximum voltage, CCCV charge mode is maintained.*
8. *Repeat the procedure from D to G for approximately 200 cycles (till capacity hits 80%).*

A summary of one fast charge aging cycle is illustrated in Fig. 1.

III. Battery Aging Model Development and Parameters Fitting

In this section, an aging model is developed and electrochemical battery model parameters for aged batteries at 80% capacity are estimated. The section is divided into two subsections as follows: Subsection *A* provides a brief summary of the reduced-order electrochemical battery model. Subsection *B* illustrates the necessity of having an updated model parameters as battery ages. This is done by assessing the performance of a model developed from a fresh battery vs. data from aged battery. Subsection *C* demonstrates the process of aging model development and model parameters evaluation as battery ages.

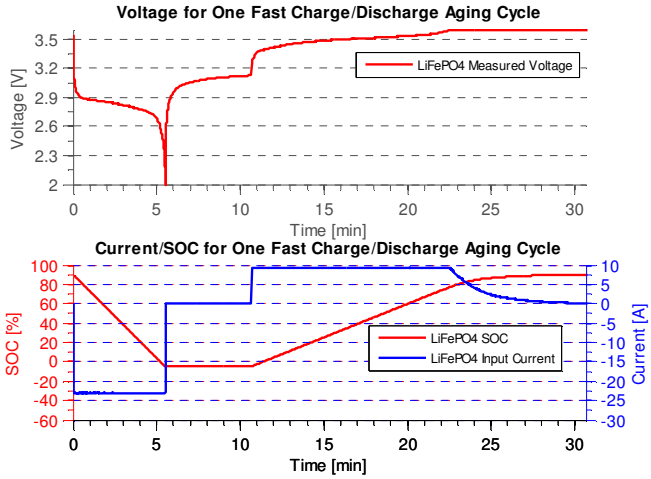

Fig. 1. Voltage, Current and SOC for One Fast Charge/Discharge Aging Test

A. Reduced-Order Electrochemical Battery Model

A detailed description of the reduced-order electrochemical battery model and the developed parameterization model can be found in [1]. A summary of the reduced-order model equations is illustrated here for the purpose of readability and completeness. Recall that each electrode can be modeled as a sphere with particle radius R_s. The single spherical particle is divided into $M_r - 1$ shells each of size Δr with $i = 1, \dots, M_r - 1$ and $r_i = i\Delta r$, where:

$$\Delta r = \frac{R_s}{M_r} \tag{1}$$

The particle outer shell (M_r) is exposed to the input current on the solid-electrolyte interface. The system, which has one input, one output, and M_{r-1} states representing the shells surface concentrations, can be summarized in the following state-space representation from [13]:

This article has been accepted for publication in a future issue of this journal, but has not been fully edited. Content may change prior to final publication. Citation information: DOI 10.1109/JESTPE.2014.2331062, IEEE Journal of Emerging and Selected Topics in Power Electronics

System equation:

$$\dot{c}_s = \begin{bmatrix} -2 & 2 & 0 & \cdots & & 0 & \\ 1/2 & -2 & 3/2 & \cdots & & 0 & \\ 0 & 2/3 & -2 & & & 0 & \\ \vdots & & & \ddots & & \vdots & \\ & & & & -2 & \frac{M_r-2}{M_r-3} & 0 \\ 0 & 0 & 0 & \cdots & \frac{M_r-3}{M_r-2} & -2 & \frac{M_r-1}{M_r-2} \\ & & & & 0 & \frac{M_r-2}{M_r-1} & \frac{2-M_r}{M_r-1} \end{bmatrix} c_s + \alpha_2 \begin{bmatrix} 0 \\ 0 \\ \vdots \\ -\left(\frac{M_r}{M_r-1}\right) \end{bmatrix} u \quad (2)$$

Output equation:

$$c_{se} = c_{s_{M_r}} = c_{s_{M_{r-1}}} - \frac{\alpha_2}{\alpha_1} J^{Li} \quad (3)$$

The model input u is the butler-Volmer current (J^{Li}) which is a function of the solid-electrolyte surface concentration (c_{se}) and the total current (I). The output of this sub-model is the solid concentration at the solid-electrolyte interface (c_{se}). This output is fed into another sub-model that calculates the terminal voltage and the state of charge. The solid-electrolyte interface concentration from the negative electrode ($c_{se,n}$) is calculated from the positive one ($c_{se,p}$) using the following equation [13]:

$$\bar{c}_{se,n} = c_{s,max,n}\left(\theta_{n0\%} + \frac{\bar{c}_{se,p} - \theta_{p0\%} c_{s,max,p}}{(\theta_{p100\%} - \theta_{p0\%}) c_{s,max,p}} (\theta_{n100\%} - \theta_{n0\%})\right) \quad (4)$$

Where $\theta_{n0\%}$, $\theta_{n100\%}$, $\theta_{p0\%}$, $\theta_{p100\%}$ are the stoichiometry points for the negative and positive electrodes, respectively [14]. The terminal voltage can be calculated based on the solid-electrolyte-interface concentrations (c_{se}) from the anode and the cathode as follows [13]:

$$V(t) = \left(\bar{\eta}_p - \bar{\eta}_n\right) + \left(\bar{\emptyset}_{e.p} - \bar{\emptyset}_{e.n}\right) + \left(U_P\left(c_{se,p}\right) - U_n\left(c_{se,n}\right)\right) - R_f I \quad (5)$$

Recall the state of charge can be calculated as [13]:

$$SOC = 100 * \left(\frac{\frac{c_{s,p_{avg}}}{c_{s,max,p}} - \theta_{p0\%}}{\theta_{p100\%} - \theta_{p0\%}}\right) \quad (6)$$

Where the average concentrations can be calculated as [13]:

$$c_{s,p_{avg}} = \frac{c_T}{V} = \frac{total\ lithium\ concetration}{particle\ volume} = \frac{\sum_{i=1}^{M_r-1} r_i^2 4\pi\Delta r}{\frac{4}{3}\pi(R_s - \Delta r)^3} \quad (7)$$

B. Aged Battery vs. Optimized ECM Model (Fresh)

In order to demonstrate the importance of having multiple battery models at various battery states of life, current profile from a UDDS driving cycle is applied to aged battery (at 80% capacity fade). The measured experimental voltage is compared against the voltage from an ECM using the optimized model parameters obtained for a fresh battery [1]. The actual SOC is obtained from the Arbin cycler using coulomb counting. The battery SOC is calculated based on the battery discharge capacity conducted as a reference performance test at the beginning of the test.

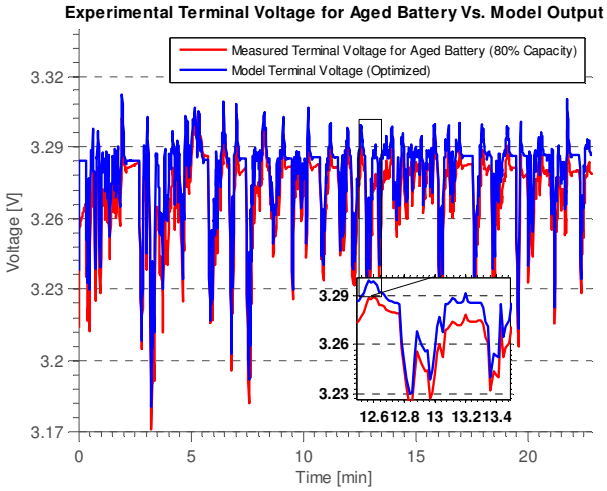

Fig. 2. Electrochemical Battery Model vs. Experimental Data from a UDDS Driving Cycle (Aged Battery)

The battery discharge capacity for the battery after the aging test is 1.74 Ah. As shown in Fig. 2 and Fig. 3, it is clear that if the same ECM fitted at 100% capacity (fresh battery) will exhibit significant deviation in both terminal voltage and SOC as battery ages.

As shown in Fig. 3, it is critical to update model parameters as battery ages since the ECM model estimate of the SOC is higher than the actual SOC which indicates a false SOC estimate. For example, at the end of the UDDS driving cycle, the model SOC is at approximately 44% while the actual SOC is at 41.5% which is a relatively significant error. It is also important to highlight that other factors such as temperature effects and cell-balancing have not been accounted for in the scope of this paper. These factors will contribute to modeling errors and uncertainties which will worsen the terminal voltage and SOC estimate.

This article has been accepted for publication in a future issue of this journal, but has not been fully edited. Content may change prior to final publication. Citation information: DOI 10.1109/JESTPE.2014.2331062, IEEE Journal of Emerging and Selected Topics in Power Electronics

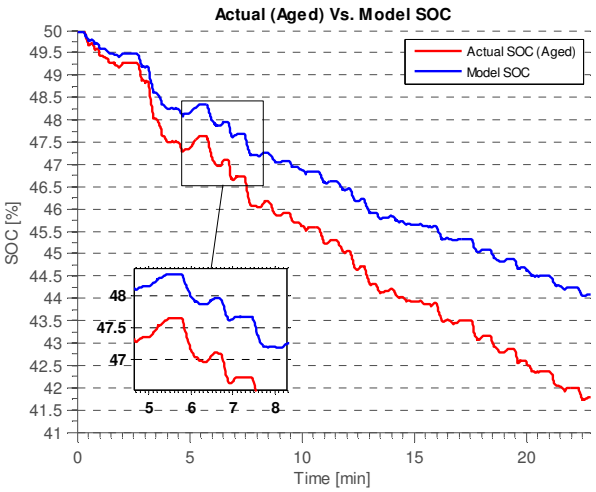

Fig. 3. Actual SOC for Aged Battery (using Coulomb Counting) vs. Model SOC

The root mean square error (RMSE) between the measured terminal voltage (V(t)) and the electrochemical model output ($\hat{V}(t)$) for n number of samples can be calculated as follows:

$$RMSE = \sqrt{\frac{\sum_{t=1}^{n} V(t) - \hat{V}(t)}{n}} \quad (8)$$

Results for both terminal voltage and the SOC are 0.0087 V and 1.4694 %, respectively. However, the model performs really well with data from healthy batteries, the RMSE of the terminal voltage and the SOC are 0.22057 mV and 0.1%. It is important to highlight that this error is over a single driving cycle which depletes the battery from 50% to approximately 40%. This error will worsen for extended driving cycles that might deplete the battery from 90% to 10%. A summary of the RMSE for the UDDS driving cycle for both fresh and aged batteries is as shown in Fig. 4. In the following section, a strategy is applied to effectively overcome this problem and account for battery aging and degradation.

C. Battery Aging Model Development

Battery aging and performance degradation occur due to two main effects, namely: film growth and carbon retreat [15]. These two phenomena are found to be changing in a sigmoidal fashion (with sudden changes after a number of cycles) [15]. Aging occurs due to the reaction between the cathode active materials and the electrolyte resulted in formation of a solid-electrolyte interface (SEI) layer which in turn changes the particle surface composition leading to breaking down of the carbon conductive path which causes carbon retreat and sudden acceleration of capacity fade [15]. Furthermore, battery aging occurs due to the formation of an insulating layer on the surface of the electrodes particles (mainly the cathode electrode) which in turn lead to increase in the impedance of the positive electrode [16]. The other factor is likely due to loss of electron conductivity of the cathode particles [17]. This phenomenon is also related to the (carbon retreat) phenomenon which is the disconnection of carbon within the particles due to the formation of a SEI layer.

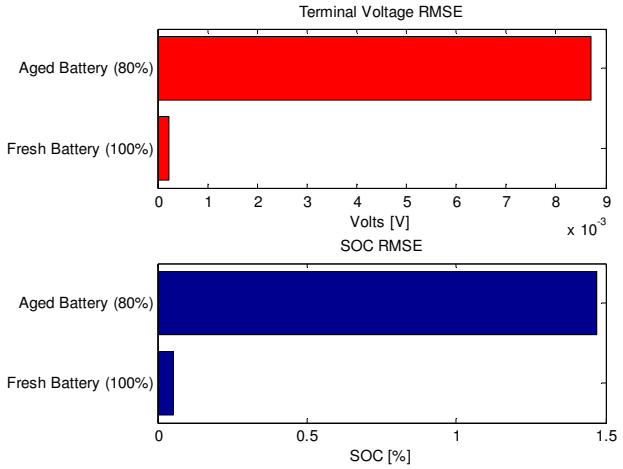

Fig. 4. Terminal Voltage RMSE for Fresh vs. Aged Battery (Upper), SOC RMSE for Fresh vs. Aged (Lower)

In order to incorporate aging into the reduced-order electrochemical model, modification to the reduced-order model has to be conducted. As shown in Fig. 5, the battery reduced-order electrochemical model at 3 distinct states of life, namely: fresh (healthy state), mid-life, and end-of-life is presented. The proposed battery aging model works by modeling the increase in the SEI layer and the decrease in the electrode volume due to side reactions. As battery ages, the electrode resistance to accept further lithium ions increases and this results in capacity degradation and aging.

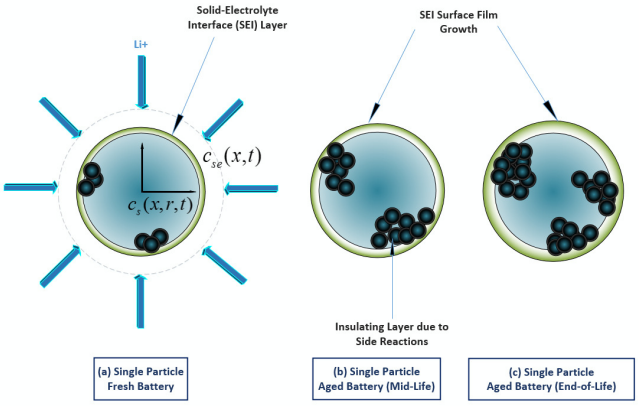

Fig. 5. Battery Reduced-order Electrochemical Model at 3 States of Life; (a) Fresh (healthy state), (b) Mid-life, and (c) End-of-life. Aging is modeled by increase in the SEI layer and decrease in the Effective Electrode Volume.

Recall that at steady state, when no further lithium diffusion occurs inside the spherical particle representing the electrode. All lithium concentrations in every shell reaches a steady state condition according to the following equation [1]:

This article has been accepted for publication in a future issue of this journal, but has not been fully edited. Content may change prior to final publication. Citation information: DOI 10.1109/JESTPE.2014.2331062, IEEE Journal of Emerging and Selected Topics in Power Electronics

$$c_i = c_T/(r_{M_{r-1}}^2 * 4\pi\Delta r) * c_{s_{factor}} = \sum_{i=1}^{M_r-1} r_i^2 4\pi\Delta r c_i /(r_{M_{r-1}}^2 * 4\pi\Delta r) * c_{s_{factor}} = (r_1^2 * 4\pi\Delta r c_1 + r_2^2 * 4\pi\Delta r c_2 + r_3^2 * 4\pi\Delta r c_3 \dots + r_{M_{r-1}}^2 * 4\pi\Delta r c_{M_r-1})/(r_{M_{r-1}}^2 * 4\pi\Delta r) * c_{s_{factor}} \quad (9)$$

where c_i represents the steady state initial concentration at every shell of the spherical particle for a given state of charge and number of shells in the particle.

In order to demonstrate the previous equation, consider a spherical particle of radius 0.0015 cm with 11 spherical discretization segments (spherical shells) and assume that the total lithium concentration is concentrated at the outermost shell. The maximum lithium concentration of 0.04782 mol/ cm^3, and assume an initial SOC of 50%. The stoichiometry values of 0.6976 and 0.9149 has been selected. By substituting with the SOC in the following equation, average lithium concentration at the specified state of charge is calculated as follows [1]:

$$c_{s,p_{avg}} = \left(\frac{SOC}{100} * (\theta_{p100\%} - \theta_{p0\%}) + \theta_{p0\%}\right) * c_{s,max,p} = 0.0386\ mol/cm^3 \quad (10)$$

Assuming the total lithium concentration is concentrated at the outermost shell, lithium concentration at the outermost shell $c_{s_{p_{M_r-1}}}$ can be calculated as follows:

$$c_{s_{p_{M_r-1}}} = c_{s,p_{avg}} * \frac{4}{3}\pi(R_s - \Delta r)^3/(r_{M_{r-1}}^2 * 4\pi\Delta r) = 0.1285\ mol/cm^3$$

As shown in Fig. 6, assuming no input current is applied at the solid-electrolyte interface layer, lithium at the outermost shell (starting from 0.1285 mol/cm^3) will diffuse inside the sphere according to Fick's second law of diffusion until all lithium concentrations are equalized, and no further lithium diffusion would occur inside the sphere. The final concentration value in which all shells settle is related to the $c_{s_{factor}}$ according to (11).

Lithium concentrations in every shell can be calculated by applying the final value theorem below:

$$c_{s_{factor}} = final\ value = \lim_{t\to 0} f(t) = \lim_{s\to 0} s((sI - A)^{-1}c(0)) = 0.2597 \quad (11)$$

The final value, which is dependent on the state transition matrix A is 0.259. It is important to highlight that this value solely depends on the number of discretization segments M_r which is 11 in this example. The steady state value of lithium concentrations, as shown in Fig. 6, can be calculated as follows:

$$c_i = c_{s_{p_{M_r-1}}} * c_{s_{factor}} = c_T/(r_{M_{r-1}}^2 * 4\pi\Delta r) * c_{s_{factor}} = 0.1285 * 0.2597 = 0.033 mol/cm^3 \quad (12)$$

Recall that the optimizer is used to optimize the electrode area (A) and then using the constraint to calculate the electrode thickness δ as follows [1]:

$$\delta = \left(\frac{1}{A}\right) * \left(\left(\frac{2M_r - 1}{2}\right) * \left(\frac{M_r}{M_r - 1}\right)^3 * \alpha_2 * \Delta r * c_{s_{factor}}\right)/(c_{s_{max}} * R_s * Q_{max} * (\theta_{p_{100\%}} - \theta_{p_{0\%}})) \quad (13)$$

This relationship is important since as battery ages, the effective volume of the sphere representing the electrode is decreased.

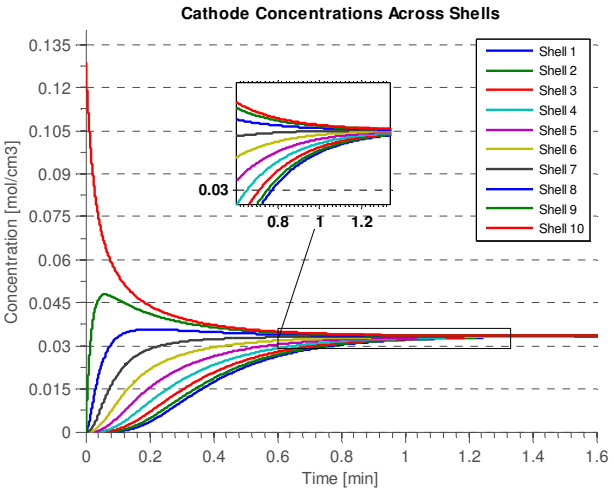

Fig. 6. Lithium concentrations across shells assuming total lithium concentration is concentrated at the outermost shell

This results in capacity degradation and battery aging. In this paper, the term *"Electrode Aging Factor* (τ)*"* is introduced as follows:

$$Electrode\ Aging\ Factor\ (\tau) = \frac{I}{J * \delta * A} = (I)/\left(J * \left(\frac{2M_r - 1}{2}\right) * \left(\frac{M_r}{M_r - 1}\right)^3 * \alpha_2 * \Delta r * c_{s_{factor}}\right)/(c_{s_{max}} * R_s * Q_{max} * (\theta_{p_{100\%}} - \theta_{p_{0\%}})) \quad (14)$$

In other words, the battery input current is scaled down to the Butler-Volmer current by dividing the input current by the effective electrode volume (V_{eff}). As battery ages, the effective electrode volume is reduced and thus lithium ions are prevented from further diffusion inside the particle representing the electrode. The effective electrode volume can be calculated as

This article has been accepted for publication in a future issue of this journal, but has not been fully edited. Content may change prior to final publication. Citation information: DOI 10.1109/JESTPE.2014.2331062, IEEE Journal of Emerging and Selected Topics in Power Electronics

follows:

$$V_{eff} = \delta * A * \tau \quad (15)$$

In order to demonstrate the presented model, assume that an input discharge current of 1C (-2.3 A) is applied for 15 minutes on the outermost shell of the sphere with the same parameters as previously discussed. Then a resting period of 15 minutes, followed by a charging current of +2.3A then a 15 minutes resting period as shown below in Fig. 7. Assume the electrode plate area is 16524.27 cm^2 and assuming the battery capacity Q_{max} is 2.3 Ah and $\alpha_2 = 1/(Fa_s\Delta r)$ is 4.632e-7.

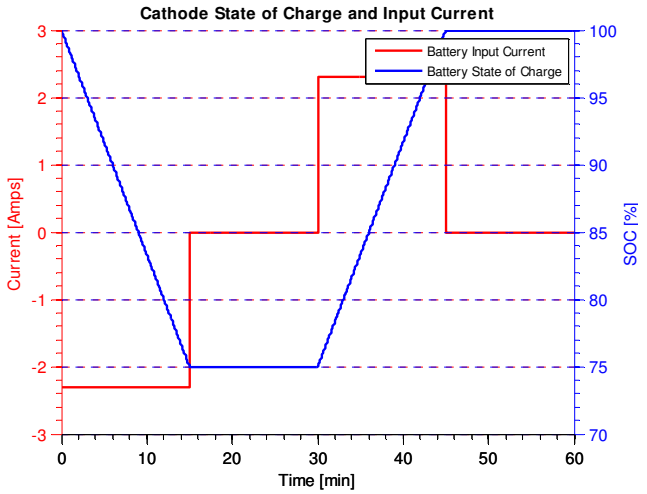

Fig. 7. Cathode Input Current and State of Charge for healthy battery (100% capacity)

Lithium ion concentrations across the particle spherical shells due to the input current are as shown in Fig. 8. It is clear that during the first 15 minutes when a discharging current is applied to the battery, lithium ion concentration across shells decrease uniformly until a steady state condition occurs. During the resting period, when no current is applied to the battery, lithium concentration equalizes across spherical shells. Lithium values is approximately 0.0356 mol/cm^3.

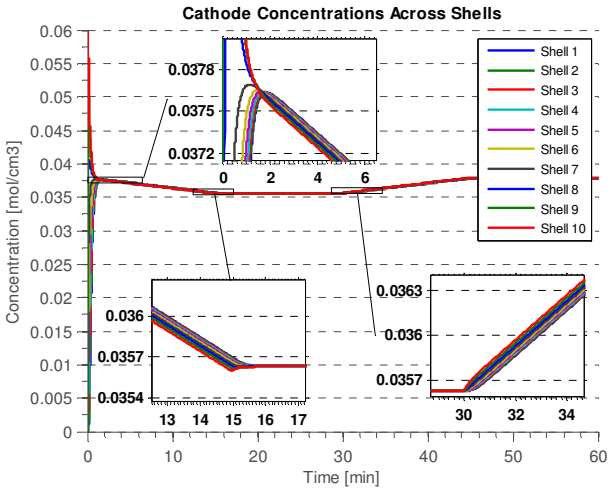

Fig. 8. Lithium Concentration variations vs. time for healthy battery (100% capacity)

During the charging period, lithium ion concentration across shells increases uniformly as shown in Fig. 8 followed by the steady-state (relaxation period). For the fresh battery, the SOC changes from 100% to 75% using the specified charging/discharging input current.

As battery degrades, the battery effective volume is decreased which in turn changes the electrode aging factor (τ). Battery aging is attributed to cycling and calendar aging effects. Calendar aging is not considered within the scope of this paper. Assume that the aging factor decreased from 1 for a fresh (healthy) battery state to 0.7 at its end of life. Other parameters such as the solid diffusion coefficient (D_{s_p}) changes as battery degrades. Changes in these parameters reflect the increased electrode resistance to accept further charges. In this example, the diffusion coefficient decreases from 7.4324e-9 to 5.34479e-9 cm^2/sec. Battery state of charge, as shown below in Fig. 9, varies from 100% to 64% using the same input current. This indicates that the electrode can no longer accepts further charges due to the change in its effective volume and decreased diffusion coefficient.

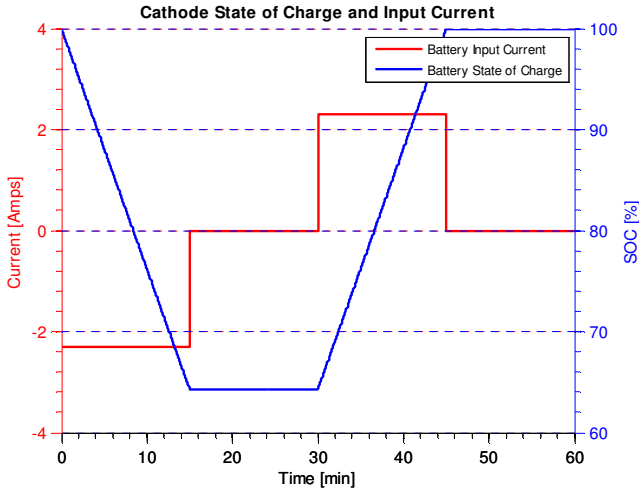

Fig. 9. Battery input current and SOC for aged battery (τ = 0.7)

As shown in Fig. 10, lithium concentrations are generally below the concentration values of a fresh battery. The steady state values of lithium concentration for a fresh battery is 0.03563 mol/cm^3, however for the aged battery, lithium concentrations at steady state is approximately 0.0346 mol/cm^3. This describes the lower state of charge values for the same current input. Regarding the battery terminal voltage, the OCV-SOC relationship changes as battery ages in addition to other parameters such as the solid-electrolyte interface resistance and the stoichiometry values for both the cathode and the anode. Variations in these parameters will be tracked using genetic algorithm optimization technique discussed in subsection *D*.

This article has been accepted for publication in a future issue of this journal, but has not been fully edited. Content may change prior to final publication. Citation information: DOI 10.1109/JESTPE.2014.2331062, IEEE Journal of Emerging and Selected Topics in Power Electronics

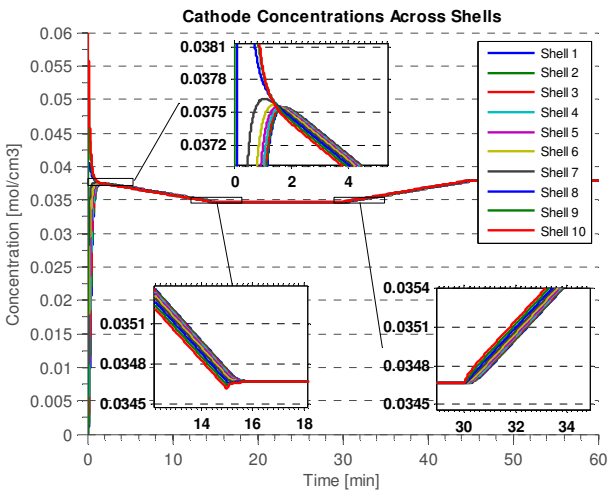

Fig. 10. Lithium Concentration variations vs. time for aged battery ($\tau = 0.7$)

D.Aging Model Parameters Optimization

In order to optimize battery model parameters as well as the electrode aging factor τ, the same optimization procedure has been conducted on aged LiFePO4 batteries at 20% capacity fade. As shown in Fig. 11, it is clear that the OCV-SOC relationship changes at various battery states of life. Since the new state of charge is defined based on the updated capacity, a shift in the SOC-OCV curve is exhibited as shown below. In order to fit the electrochemical model to aged batteries, the battery discharge capacity is updated from 2.3Ah to 1.76Ah based on the static capacity test. The genetic algorithm procedure discussed is conducted again to update model parameters for aged batteries [1].

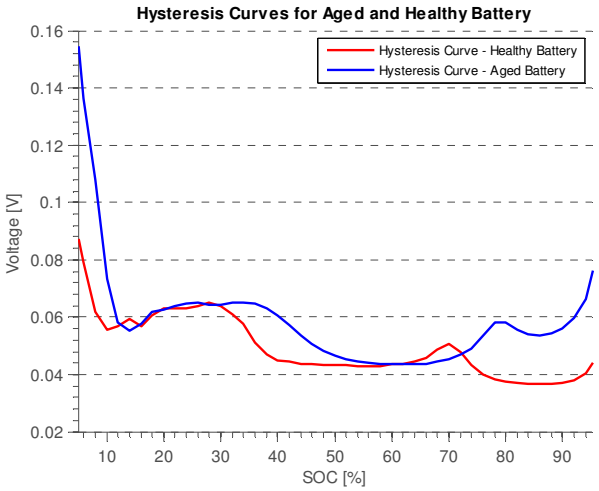

Fig. 11. SOC-OCV Hysteresis Curve for Healthy and Aged Batteries

Results for optimized battery parameters are summarized in Table 1. The terminal voltage and SOC for the updated model vs. experimental data from aged batteries are as shown in Fig. 12 and Fig. 13.

During optimization, parameters initial values are set to those of fresh batteries and the same bounds are set. Some parameters are held constant by the optimizer as follows: the solid maximum particle concentration in the anode and cathode ($c_{s,max,p}, c_{s,max,n}$), positive and negative electrode area (A), anode and cathode particle radius (R_{s_p}, R_{s_n}), active material volume fraction ($e_{s,p}, e_{s,n}$), positive and negative active surface area per electrode ($a_{s,p}, a_{s,n}$), positive and negative current coefficient or reaction rate (k_0), and average electrolyte concentration ($\bar{c}_e$). The following parameters are adjusted by the optimizer for aged batteries: electrode aging factor (τ), positive and negative diffusion coefficients ($D_{s,p}, D_{s,n}$), electrode film resistance (R_{SEI}) (also known as the solid electrolyte interface resistance), maximum positive and negative solid normalized concentrations (stoichiometry values) ($\theta_{p_{100}}, \theta_{n_{100}}$), minimum positive and negative normalized solid concentration ($\theta_{p_0}, \theta_{n_0}$).

TABLE 1.
ELECTROCHEMICAL BATTERY MODEL OPTIMIZED PARAMETERS FOR AGED BATTERIES

PARAMETER NAME (ELECTRODE) (SYMBOL) (UNIT)	OPTIMIZED PARAMETERS
Electrode aging factor (τ)	0.69
Solid phase diffusion coefficient (Positive) ($D_{s,p}$) (cm^2/sec)	5.34479 e-09
Solid phase diffusion coefficient (Negative) ($D_{s,n}$) (cm^2/sec)	1.139458 e-09
Maximum solid concentration (Positive) ($\theta_{p_{100\%}}$)	0.91496
Minimum solid concentration (Positive) ($\theta_{p_{0\%}}$)	0.685320
Maximum solid concentration (Negative) ($\theta_{n_{100\%}}$)	0.499761
Minimum solid concentration (Negative) ($\theta_{n_{0\%}}$)	0.153574
Solid Electrolyte interface Resistance (R_{SEI}) (Ω)	0.011

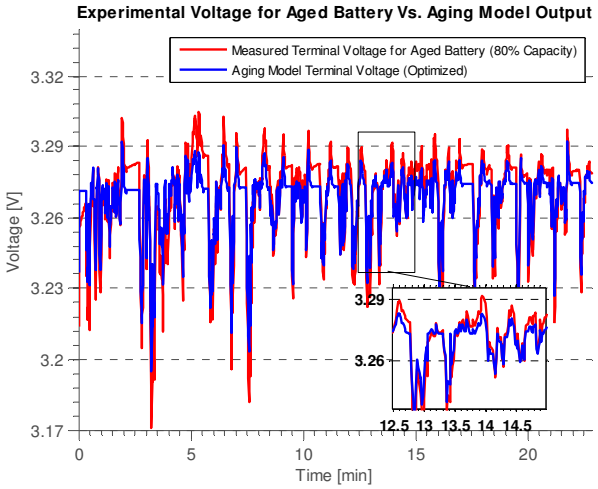

Fig. 12. Electrochemical Battery Aging Model vs. Experimental Data from a UDDS Driving Cycle (Aged Battery)

The overall RMSE using UDDS driving cycle is 0.166 mV and the SOC RMSE is 0.2029 %. As shown in Table 1, the

This article has been accepted for publication in a future issue of this journal, but has not been fully edited. Content may change prior to final publication. Citation information: DOI 10.1109/JESTPE.2014.2331062, IEEE Journal of Emerging and Selected Topics in Power Electronics

optimized electrode aging factor is less than one indicating a reduced effective electrode volume. The solid-electrolyte interface resistance increases as battery ages which indicates more resistance to lithium diffusion inside the representative particle. Stoichiometry values for both the cathode and the anode change since the OCV-SOC relationship changes with aging. The positive solid particle diffusion coefficient decreases indicating decreased rate of lithium diffusion inside the particle. Future research involves tracking changes of these parameters using correlation with ampere-hour throughput and aging parameters such as battery discharge rate, temperatures, and depth of discharge.

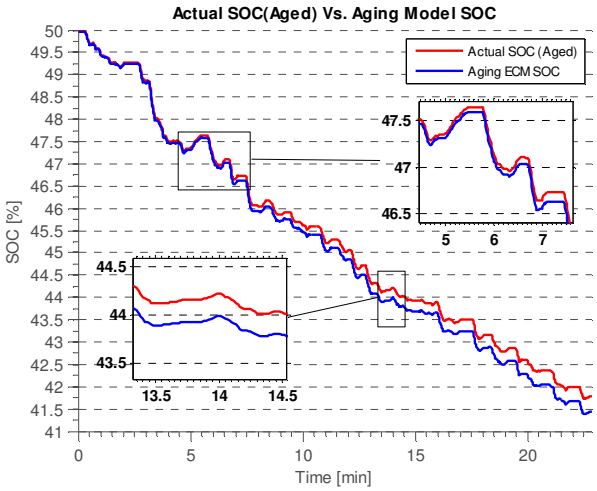

Fig. 13. Electrochemical Battery Aging Model SOC vs. Experimental Data from a UDDS Driving Cycle (Aged Battery)

IV. Battery Critical Surface Charge Estimation

In this section, an estimation strategy known as the Smooth Variable Structure Filter (SVSF) which was recently introduced in 2007 have been applied to estimate the battery critical surface charge based on the reduced-order electrochemical battery model. The following subsection (*A*) involves a brief overview of the SVSF and subsection (*B*) discusses the application of the filter to the model for critical surface charge estimation.

A. The Smooth Variable Structure Filter

Similar to Kalman filter, the SVSF works in a predictor-corrector fashion [18]. The filter is based on sliding mode concept and has demonstrated robustness to modeling uncertainties and sensor noise [18, 8]. The SVSF can be applied to both linear and non-linear systems. It works by using an SVSF gain that forces the states to converge to the boundary of the true (desired) state estimates [18]. The gain forces the states to switch back and forth across the state trajectory within a region referred to as the existence subspace which is function of the model uncertainties. The width of the existence space β is a function of the uncertain dynamics associated with the inaccuracy of the internal model of the filter as well as the measurement model, and varies with time [18]. The SVSF can be applied to systems that are differentiable and observable [18, 19]. The original form of the SVSF as presented in [18] did not include covariance derivations. An augmented form of the SVSF was presented in [20], which includes a full derivation for the filter.

Consider the nonlinear system with linear output (measurement) equation. The filter run by generating a prediction of the state estimate (which represents the solid-electrolyte interface concentration) as follows:

$$\hat{x}_{k+1|k} = \hat{f}(\hat{x}_{k|k}, u_k) \tag{16}$$

The predicted estimates are then used to generate a predicted measurements $\hat{z}_{k+1|k}$ as follows [18]:

$$\hat{z}_{k+1|k} = C_{k|linearized}\hat{x}_{k+1|k} \tag{17}$$

Where $C_{k|linearized}$ is the measurement matrix. Then the measurement error $e_{z,k+1|k}$ can be calculated as follows [18]:

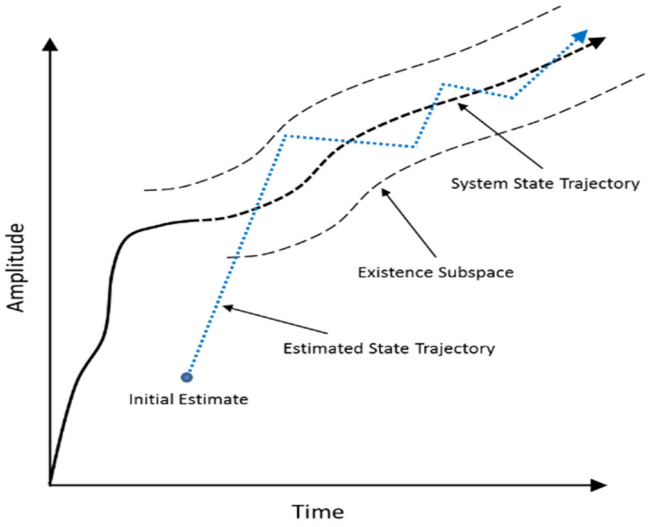

Fig. 14. The SVSF estimation strategy starting from some initial value, the state estimate is forced by a switching gain to within a region referred to as the existence subspace [18].

$$e_{z,k+1|k} = z_{k+1} - \hat{z}_{k+1|k} \tag{18}$$

The SVSF gain is a function of the a-priori and the a-posteriori measurement errors $e_{z_{k+1|k}}$ and $e_{z_{k|k}}$, the smoothing boundary layer widths ψ, the 'SVSF' memory or convergence rate γ, as well as the linear measurement matrix $C_{k|linearized}$. For the derivation of the SVSF gain K_{k+1}, refer to [18, 20]. The SVSF gain may be defined diagonally as follows [18]:

$$\begin{aligned} K_{k+1} &= C_{k|linearized}{}^{+} diag\left[\left(\left|e_{z_{k+1|k}}\right| + \gamma\left|e_{z_{k|k}}\right|\right)\right. \\ &\left. \circ\, sat\left(\frac{e_{z_{k+1|k}}}{\psi}\right)\right] diag\left(e_{z_{k+1|k}}\right)^{-1} \end{aligned} \tag{19}$$

The updated states $\hat{x}_{k+1|k+1}$ are calculated as follows [18]:

$$\hat{x}_{k+1|k+1} = \hat{x}_{k+1|k} + K_{k+1}e_{z_{k+1|k}} \tag{20}$$

Calculation of a posteriori output estimate $\hat{z}_{k+1|k+1}$ and

This article has been accepted for publication in a future issue of this journal, but has not been fully edited. Content may change prior to final publication. Citation information: DOI 10.1109/JESTPE.2014.2331062, IEEE Journal of Emerging and Selected Topics in Power Electronics

measurement errors $e_{z_{k+1|k+1}}$ are calculated afterwards. The output estimates and a posteriori measurement errors are calculated respectively as follows [18]:

$$\hat{z}_{k+1|k+1} = C_{k|linearized}\hat{w}_{k+1|k+1} \tag{21}$$

$$e_{z_{k+1|k+1}} = z_{k+1} - \hat{z}_{k+1|k+1} \tag{22}$$

Equations 17 to 22 are iteratively repeated until a certain threshold is attained. As per [18], the estimation process is stable and convergent if the following lemma is satisfied:

$$\left|e_{k|k}\right| > \left|e_{k+1|k+1}\right| \tag{23}$$

The proof, as defined in [18], yields the derivation of the SVSF gain from (26). The standard SVSF gain yields the following:

$$e_{z,k+1|k+1} = e_{z,k+1|k} - HK_{k+1} \tag{24}$$

Substitution of (24) into (23) yields:

$$\left|e_{z,k|k}\right| > \left|e_{z,k+1|k} - HK_{k+1}\right| \tag{25}$$

Simplifying and rearranging (28):

$$|HK_{k+1}| > \left|e_{z,k+1|k}\right| + \gamma\left|e_{z,k|k}\right| \tag{26}$$

Based on the fact that $|\mathrm{HK_{k+1}}| = \mathrm{HK_{k+1}} \circ \mathrm{sign}(\mathrm{HK_{k+1}})$, the standard SVSF gain can be derived as follows:

$$K_{k+1} = H^{-1}\left(\left|e_{z,k+1|k}\right| + \gamma\left|e_{z,k|k}\right|\right) \circ sign(HK_{k+1}) \tag{27}$$

Equation (27) may be further expanded based on the fact that $\mathrm{sign}(\mathrm{HK_{k+1}}) = \mathrm{sign}(\mathrm{e_{z,k+1|k}})$, as per [18], such that:

$$K_{k+1} = H^{-1}\left(\left|e_{z,k+1|k}\right| + \gamma\left|e_{z,k|k}\right|\right) \circ sign\left(e_{z,k+1|k}\right) \tag{28}$$

The SVSF switching may be smoothed out by the use of a saturation function, accordingly, (28) becomes:

$$K_{k+1} = H^{-1}\left(\left|e_{z,k+1|k}\right| + \gamma\left|e_{z,k|k}\right|\right) \circ sat\left(e_{z,k+1|k}\right) \tag{29}$$

where the saturation function is defined by:

$$sat\left(e_{z,k+1|k}\right) = \begin{cases} 1, & e_{z,k+1|k} \geq 1 \\ e_{z,k+1|k}, & -1 < e_{z,k+1|k} < 1 \\ -1, & e_{z,k+1|k} \leq -1 \end{cases} \tag{30}$$

Finally, a smoothing boundary layer ψ may be added to further reduce the magnitude of chattering, leading to:

$$K_{k+1} = H^{-1}\left(\left|e_{z,k+1|k}\right| + \gamma\left|e_{z,k|k}\right|\right) \circ sat\left(e_{z,k+1|k}/\psi\right) \tag{31}$$

Note that the gain described in (31) is slightly different than that presented earlier in (19). A diagonalized form was created, as described in [20, 21], to formulate an SVSF derivation that included a covariance function. The form shown as (31) was presented as the original or 'standard' SVSF in [18].

B. SVSF-based Critical Surface Charge Estimation-fresh battery

The SVSF has been used to estimate the critical surface charge based on the reduced-order model. The state space representation indicating the diffusion of lithium into the solid particle consists of a linear system (3) and a nonlinear measurement (output) (5). The terminal voltage is function of the solid-electrolyte interface concentrations $\mathrm{c_{se,p}}$ and $\mathrm{c_{se,n}}$. The model has one input current (I), $\mathrm{M_r} - 1$ states and, and one output representing the terminal voltage ($\mathrm{V_T}$). The measured voltage is compared to the model output to calculate the error signal that is fed back to the SVSF estimator to calculate the gain and update the states. The output equation is linearized with respect to the current state as follows:

$$C_{k|linearized} = \frac{\partial V}{\partial x} = \frac{\partial \mathrm{V}}{\partial \bar{\mathrm{c}}_{\mathrm{s,p(M_r-1)}}} \tag{32}$$

Due to the complexity of the output equation, complex differentiation has been conducted to linearize the output equation then to generate the $\mathrm{C_{k|linearized}}$ matrix. The $\mathrm{C_{k|linearized}}$ matrix consists of zero elements except for the last element thus when used to update the states, only the solid electrolyte interface concentration is updated.

The filter can estimate the solid-electrolyte interface concentration $\mathrm{c_{se,p}}$ and since at steady state conditions, all lithium concentrations are equalized (no further diffusion occurs), the filter can estimate all the spherical shell concentrations and thus provides an estimate of the initial SOC. Accordingly, the filter can be used to estimate the SOC at steady state conditions to correct the initial SOC then the model takes over as shown below.

It is important to shortly discuss computational issues that may occur when calculating the pseudoinverse of the linearized measurement matrix in (19). Numerous authors have experienced abrupt and unexpected instabilities with the pseudoinverse [22, 23]. A sudden growth of the Jacobian matrix elements when calculating the pseudoinverse during the SVSF gain calculation occurs at each iteration. Consequently, the estimator outputs and thus the mean square error between the measured terminal voltage and model output increases significantly. A stabilizing adjustment is performed to avoid this problem. The problem has been extensively analyzed in [22], and occurs due to the presence of singularities. Singularities occur when the Jacobian matrix loses rank. Small singular values of H might arise in the vicinity of these singularities. Consequently, larger values occur when obtaining

This article has been accepted for publication in a future issue of this journal, but has not been fully edited. Content may change prior to final publication. Citation information: DOI 10.1109/JESTPE.2014.2331062, IEEE Journal of Emerging and Selected Topics in Power Electronics

the pseudoinverse of the Jacobian H^+ thus creating larger error values which leads to instability. According to [24], it is rather difficult to detect these singularities. A traditional method of solving this instability problem is by replacing the pseudoinverse H^+ with the following equation [24]:

$$C_d^+ = C^T(CC^T + \rho^2 I)^{-1} \quad (36)$$

where, ρ is called the damping parameter. The effect of the added damping is that it mitigates the effect of small singular values when computing the inverse [24]. On the other hand, a slightly small error is introduced when calculating the inverse. In this paper, ρ is set to 0.4, and is shown to have a negligible effect on the accuracy. As shown in Fig. 15, 16 and 17, the SVSF estimation strategy has been applied to estimate the critical surface concentration, the battery state of charge, and the battery terminal voltage for zero input current. The battery actual state of charge is held at 34% and the estimator is initialized at 50% SOC which is a relatively large deviation. Since all battery states are held at steady state conditions, the battery SOC and terminal voltage can be estimated accordingly with high accuracy.

The estimation error for both the terminal voltage and the SOC are as shown in Fig. 17. It is clear that the SOC estimator converges to the actual SOC value within approximately 2-3 minutes assuming the initial SOC is at 47% error from the actual SOC which is a significantly large error. The estimator converges much faster if the initial SOC is close to the actual SOC values. Furthermore, the SVSF estimation capability have been tested using an aggressive driving cycle that entails fast acceleration and regenerative braking. Current profile from a US06 driving cycle has been used for testing. Estimated vs. experimental voltage are as shown in Fig. 18.

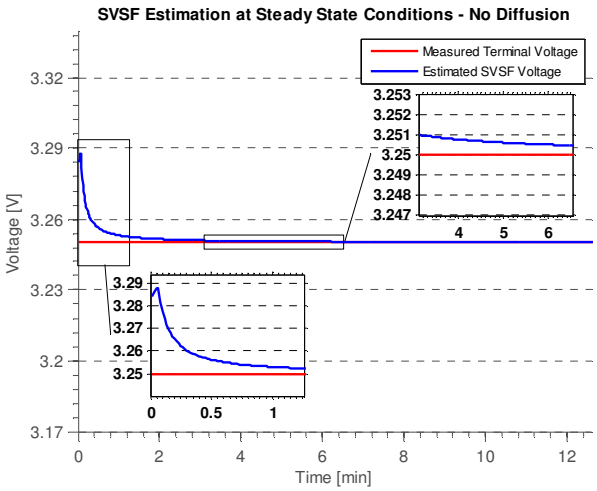

Fig. 15. SVSF Voltage Estimation at steady state conditions - equal lithium concentrations across shells

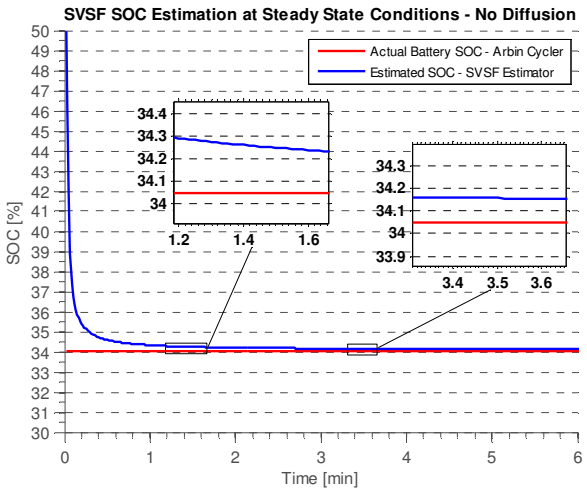

Fig. 16. SVSF SOC Estimation at steady state conditions - equal lithium concentrations

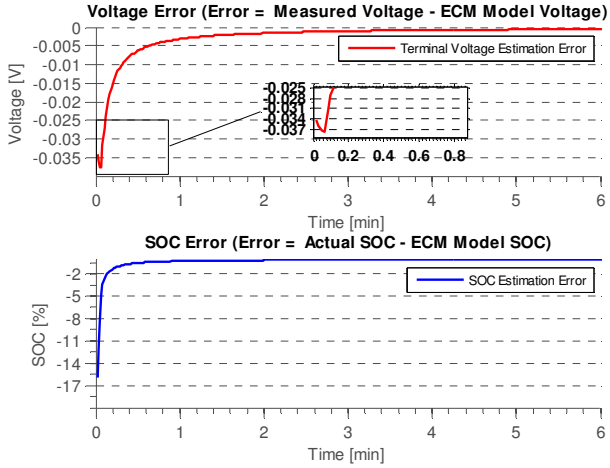

Fig. 17. Terminal Voltage Estimation Error (Upper) and the SOC Estimation Error (Lower)

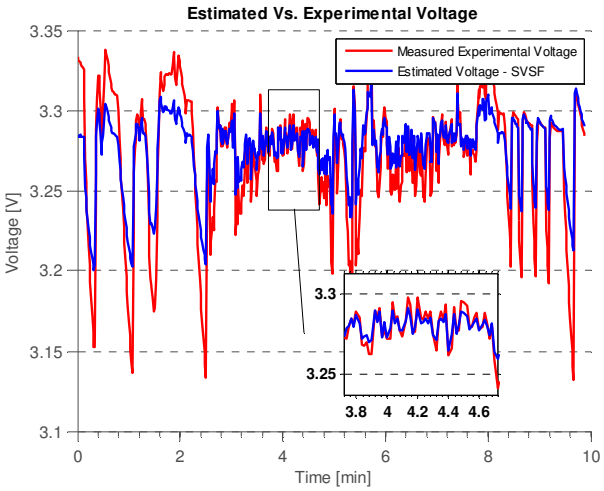

Fig. 18. SVSF Estimated Voltage Vs. Experimental Data

The electrochemical model SOC vs. experimental SOC (using coulomb counting from Arbin Cycler) is as shown below in Fig. 19.

This article has been accepted for publication in a future issue of this journal, but has not been fully edited. Content may change prior to final publication. Citation information: DOI 10.1109/JESTPE.2014.2331062, IEEE Journal of Emerging and Selected Topics in Power Electronics

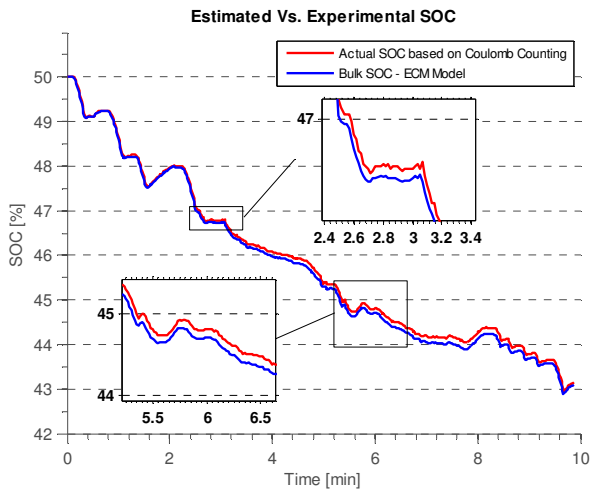

Fig. 19. ECM Model SOC vs. Experimental (Coulomb Counting) SOC

The terminal voltage and SOC estimation error for US06 driving cycle are as shown below in Fig. 20. The maximum error in the SOC is within 0.2 % and within 0.05V for the terminal voltage. The RMSE for the SOC is 0.0989% and 0.0207V for the terminal voltage, respectively.

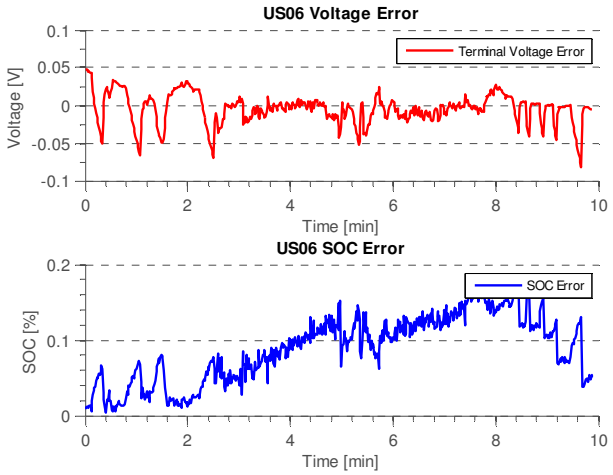

Fig. 20. US06 Voltage (Upper) and SOC (Lower) Error

V. Conclusion

The paper extends on the existing electrochemical battery models to accommodate for aging and degradation that occurs overtime. An aging battery model is developed by changing the effective electrode volume to model capacity degradation. A non-invasive genetic algorithm has been applied to estimate model parameters for aged batteries. Main parameters that contribute to battery aging are: the OCV-SOC relationship, the solid-electrolyte interface resistance (c_{se_p}), the solid diffusion coefficient (D_s), the electrode effective volume (τ), and the minimum and maximum stoichiometry values ($\theta_{p_{0\%}}$) and ($\theta_{p_{100\%}}$). The battery loss of capacity due to aging is attributed to the increase in the battery solid electrolyte interface resistance, the decrease in diffusion coefficient, and the decrease in the battery electrode effective volume, those changes reflect the electrode tendency to resist further lithium diffusion as battery degrades.

Extensive accelerated aging and reference performance tests have been conducted on lithium-iron phosphate cells. Reference tests have been conducted at two distinct states of life, namely: 100% and 80% capacity. Furthermore, a critical state of charge estimation strategy has been implemented using the SVSF estimation methodology. Results indicate that the SVSF is robust, accurate, and reliable, and can be used for real-time applications on board of an electric vehicle battery management system. The estimator can be used to estimate the critical surface charge and the battery overall state of charge at steady state conditions. Future research involves extending the reduced-order electrochemical model to work at higher C-rates in addition to extending the strategy to the pack level.

VI. Acknowledgments

Financial support from Ford Motor Company and NSERC (National Sciences and Engineering Research Council of Canada) is gratefully acknowledged.

Table 2.
Electrochemical Battery Model Parameters Nomenclature and Units

Symbol	Name	Unit
$\mathbf{i_e}$	Electrolyte current density	A cm^{-2}
$\mathbf{i_e}$	Solid current density	A cm^{-2}
$\mathbf{\emptyset_e}$	Electrolyte potential	V
$\mathbf{\emptyset_s}$	Solid potential	V
$\mathbf{c_e}$	Electrolyte concentration	mol cm^{-3}
$\mathbf{c_s}$	Solid concentration	mol cm^{-3}
$\mathbf{c_{se}}$	Concentration at the solid electrolyte interface	mol cm^{-3}
$\mathbf{J_{Li}}$	Butler-Volmer current	A cm^{-3}
$\mathbf{\theta_n}$	Anode Normalized solid concentration	-
$\mathbf{\theta_p}$	Cathode Normalized solid concentration	-
$\mathbf{U}$	Open circuit potential	V
$\mathbf{U_n}$	Anode open circuit voltage	V
$\mathbf{U_p}$	Cathode open circuit voltage	V
$\mathbf{\eta}$	Overpotential	V
$\mathbf{F}$	Faraday's constant	C mol^{-1}
$\mathbf{I}$	Applied battery cell current	A
$\mathbf{R}$	Universal Gas constant	J K^{-1} mol^{-1}
$\mathbf{T}$	Temperature	K

VII. Bibliography

[1] R. Ahmed, M. El Sayed, J. Tjong and S. Habibi, "Reduced-Order Electrochemical Model Parameters Identification and Critical Surface Charge Estimation for Healthy and Aged Li-Ion Batteries, Part I: Parameterization Model Development for Healthy Battery," *Journal of Emerging Technologies,* 2014.

[2] S. E. Samadani, R. A. Fraser and M. Fowler, "A Review Study of Methods for Lithium-ion Battery Health Monitoring and Remaining Life Estimation in Hybrid Electric Vehicles," *SAE International* , 2012.

[3] B. Pattipati, C. Sankavaram and K. R. Pattipati, "System Identification and Estimation Framework for Pivotal Automotive Battery Management System Characteristics," *IEEE Transactions on Systems, Man, and Cybernetics,* vol. 41, no. 6, 2010.

[4] "www.mynissanleaf.com/wiki/," [Online].

[5] K. A. Smith, C. D. Rahn and C.-Y. Wang, "Model-Based Electrochemical Estimation of Lithium-Ion Batteries," in *IEEE International Conference on Control Applications*, San Antonio, Texas, USA, September 3-5, 2008.

[6] R. Klein, N. A. Chaturvedi, J. Christensen, J. Ahmed, R. Findeisen and A. Kojic , "Electrochemical Model Based Observer Design for a Lithium-Ion Battery," *IEEE Transactions on Control Systems Technology,* vol. 21, no. 2, 2013.

[7] H. Rahimi-Eichi, F. Baronti and M.-Y. Chow, "Modeling and Online Parameter Identification of Li-Polymer Battery Cells for SOC estimation," in *IEEE International Symposium on Industrial Electronics (ISIE)*, Hangzhou, 2012.

[8] S. R. Habibi and R. Burton, "The Variable Structure Filter," *Journal of Dynamic Systems, Measurement, and Control (ASME),* vol. 125, pp. 287-293, September 2003.

[9] S. R. Habibi and R. Burton, "Parameter Identification for a High Performance Hydrostatic Actuation System using the Variable Structure Filter Concept," *ASME Journal of Dynamic Systems, Measurement, and Control,* 2007.

[10] M. Conte, V. C. Fiorentino , I. D. Bloom, K. Morita, T. Ikeya and J. R. Belt, "Ageing Testing Procedures on Lithium Batteries in an International Collaboration Context," China, November, 2010.

[11] "Battery Test Manual for Plug-In Hybrid Electric Vehicles," U.S. Department of Energy, Idaho National Laboratory, Idaho Falls, Idaho 83415, March 2008.

[12] G. Pistoia, Electric and Hybrid Vehicles, Rome, Italy: Elsevier, 2010.

[13] D. Domenico, S. Anna and F. Giovanni, "Lithium-Ion Battery State of Charge and Critical Surface Charge Estimation Using an Electrochemical Model-Based Extended Kalman Filter," *Journal of Dynamic Systems, Measurement, and Control,* vol. 132, pp. 1-11, 2010.

[14] D. D. Domenico, G. Fiengo and A. Stefanopoulou, "Lithium-Ion battery State of Charge estimation with a Kalman Filter based on a electrochemical model," *IEEE Interantional Conference on control Applications (CCA),* pp. 702-707, 2008.

[15] M. Dubarry, V. Svoboda, R. Hwu and B. Y. Liaw, "Capacity and power fading mechanism identification from a commercial cell evaluation," *Journal of Power Sources,* 2006.

[16] D. Abraham, R. Twesten, M. Balasubramanian, I. Petrov, J. McBreen and K. Amine, "Surface changes on LiNi0:8Co0:2O2 particles during testing of high-power lithium-ion cells," *Electrochemistry Communications,* vol. 4, pp. 620 - 625, 2002.

[17] R. Kostecki and F. McLarnon, "Degradation of LiNi0.8Co0.2O2 Cathode Surfaces in High-Power Lithium-Ion Batteries," *Electrochemical and Solid-State Letters,* vol. 5, pp. A164-A166, 2002.

[18] S. R. Habibi, "The Smooth Variable Structure Filter," *Proceedings of the IEEE,* vol. 95, no. 5, pp. 1026-1059, 2007.

[19] M. Al-Shabi, "The General Toeplitz/Observability SVSF," Hamilton, Ontario, 2011.

[20] S. A. Gadsden and S. R. Habibi, "A New Form of the Smooth Variable Structure Filter with a Covariance Derivation," in *IEEE Conference on Decision and Control*, Atlanta, Georgia, 2010.

[21] S. A. Gadsden, "Smooth Variable Structure Filtering: Theory and Applications," Hamilton, Ontario, 2011.

[22] K. O'Neil and C. Y.-C, "Instability of Pseudinverse Acceleration Control of Redundant Mechanisms," *Proceedings of the IEEE International Conference on Robotocs and Automation ,* April 2000.

[23] K. Doty, C. Melchiorri and C. Bonivento, "A theory oof generalized inverses applied to robotics," *International Robotics Journal,* vol. 12, pp. 1-19, 1993.

[24] H. Lipkin and P. E. , "Enumeration of singular configuration for robotic manipulators," *journal of Mech. Design ,* vol. 113, no. 3, pp. 272-279, 1991.

Ryan is currently a PhD candidate at McMaster University, Canada. Ryan obtained his Masters of Applied Science (M.A.Sc) degree from McMaster University. Ryan has been active in the area of hybrid vehicles control, engine management and fault detection, and battery monitoring and control. Ryan was the recipient of best paper award at the IEEE Transportation Electrification Conference and Expo (ITEC 2012), Michigan, USA. He is currently a Stanford Certified Project Manager (SCPM), certified Professional Engineer (P.Eng.) in Ontario, a member of the Green Auto Powertrain (GAPT) research team, and a student member of the Institute of Electrical and Electronics Engineers (IEEE).

Dr. Mohammed El Sayed obtained a B.Sc. in Mechanical Engineering from Helwan University, Egypt in 1999. He then earned a M.Sc. degree in Mechanical Engineering in 2003. Mohammed obtained his Ph.D. in 2012 in the areas of control theory and applied mechatronics. He is currently a registered member of the Professional Engineers of Ontario (PEO) and is currently working as a development engineer at Schaeffler Group, USA. Mohammed's research interests include: fluid power and hydraulics, state and parameter estimation, intelligent and multivariable control, actuation systems, and fault detection and diagnosis.

Ienkaran Arasaratnam received the B.Sc. degree (with first class honors) from the Department of Electronics and Telecommunication Engineering, University of Moratuwa, Sri Lanka, in 2003 and the M.A.Sc. and Ph.D. degrees from the Department of Electrical and Computer Engineering, McMaster University, Hamilton, ON, Canada, in 2006 and 2009, respectively. During his Ph.D., he developed the Cubature Kalman Filtering Algorithm for approximate nonlinear Bayesian estimation and patented its application to cognitive tracking radar systems. He is currently working as a Research and Development Engineer at Ford Motor Company in Windsor, ON, Canada. His current research focuses on electrified and intelligent transportation and energy harvesting technology.

Dr. Jimi Tjong is the Technical Leader and Manager of the Powertrain Engineering, Research & Development Centre (PERDC). It is a result oriented organization capable of providing services ranging from the definition of the problem to the actual design, testing, verification, and finally the implementation of solutions or

measures. The Centre is currently the hub for Engineering, Research and Development that involved Canadian Universities, Government Laboratories, Canadian automotive parts and equipment suppliers. The Centre includes16 research and development test cells, prototype machine shop, PHEV, HEV and BEV development testing which occupies an area of 200,000 sq ft. The Centre is the hub for Production / Design Validation of engines manufactured in North America and an overflow for the Ford worldwide facilities. It also establishes a close link worldwide within Ford Research and Innovation Centre, Product Development and Manufacturing Operations that can help bridge the gap between laboratory research and the successful commercialization and integration of promising new technologies into the product development cycle.

His principal field of Research and Development encompasses the following: Optimizing Automotive Test systems for cost, performance and full compatibility. It includes the development of test methodology and cognitive systems; Calibration for internal combustion engines; Alternate fuels, bio fuels, lubricants and exhaust fluids; Lightweight materials with the focus on Aluminum, Magnesium, bio materials; Battery, Electric motors, super capacitors, stop/start systems, HEV, PHEV, BEV systems; Nano sensors and actuators; High performance and racing engines; Non-destructive monitoring of manufacturing and assembly processes; and Advanced gasoline and diesel engines focusing in fuel economy, performance and cost opportunities.

He has published and presented numerous technical papers in the above fields internationally. Dr. Tjong is also an Adjunct Professor of the University of Windsor, McMaster University, and University of Toronto. He continuously mentors graduate students in completing the course requirements as well as career development coaching.

Dr. Saeid Habibi is currently the Director of the Centre for Mechatronics and Hybrid Technology and a Professor in the Department of Mechanical Engineering at McMaster University. Saeid obtained his Ph.D. in Control Engineering from the University of Cambridge, U.K. His academic background includes research into intelligent control, state and parameter estimation, fault diagnosis and prediction, variable structure systems, and fluid power. The application areas for his research have included aerospace, automotive, water distribution, robotics, and actuation systems. He spent a number of years in industry as a Project Manager and Senior Consultant for Cambridge Control Ltd, U.K., and as Senior Manager of Systems Engineering for AlliedSignal Aerospace Canada. He received two corporate awards for his contributions to the AlliedSignal Systems Engineering Process in 1996 and 1997. He was the recipient of the Institution of Electrical Engineers (IEE) F.C. Williams best paper award in 1992 for his contribution to variable structure systems theory. He was also awarded an NSERC Canada International Postdoctoral Fellowship that he held at the University of Toronto from 1993 to 1995, and more recently a Boeing Visiting Scholar sponsorship for 2005. Saeid is on the Editorial Board of the Transactions of the Canadian Society of Mechanical Engineers and is a member of IEEE, ASME, and the ASME Fluid Power Systems Division Executive Committee.